Multiorbital Nature of Doped Sr_2IrO_4

Guoren Zhang[1,2] and Eva Pavarini[3,4]

[1]*School of Sciences, Nantong University, Nantong, 226019, People's Republic of China*
[2]*Key Laboratory of Materials Physics, Institute of Solid State Physics, HFIPS, Chinese Academy of Sciences, Hefei 230031, People's Republic of China*
[3]*Institute for Advanced Simulation, Forschungszentrum Jülich, 52425 Jülich, Germany*
[4]*JARA High-Performance Computing, Forschungszentrum Jülich, 52425 Jülich, Germany*

The low-energy $j_{eff} = 1/2$ band of Sr_2IrO_4 bears stark resemblances with the $x^2 - y^2$ band of La_2CuO_4, and yet no superconductivity has been found so far by doping Sr_2IrO_4. Behind such a behavior could be inherent failures of the $j_{eff} = 1/2$ picture, in particular when electrons or holes are introduced in the IrO_2 planes. In view of this, here we reanalyze the $j_{eff} = 1/2$ scenario. By using the local-density approximation plus dynamical mean-field theory approach, we show that the form of the effective $j_{eff} = 1/2$ state is surprisingly stable upon doping. This supports the $j_{eff} = 1/2$ picture. We show that, nevertheless, Sr_2IrO_4 remains in essence a multiorbital system: The hybridization with the $j_{eff} = 3/2$ orbitals sizably reduces the Mott gap by enhancing orbital degeneracy, and part of the holes go into the $j_{eff} = 3/2$ channels. These effects cannot be reproduced by a simple effective screened Coulomb repulsion. In the optical conductivity spectra, multiorbital processes involving the $j_{eff} = 3/2$ states contribute both to the Drude peak and to relatively low-energy features.

In Sr_2IrO_4 low-energy electronic properties are believed to be largely determined by the effective half-filled $j_{eff} = 1/2$ band [1–4]. Support for this picture comes, experimentally, from angle-resolved photoemission [1], optical conductivity, x-ray absorption [1], and resonant x-ray magnetic scattering [2] measurements and, theoretically, from local-density approximation plus Hubbard U (LDA + U) [1,3] and dynamical mean-field theory (DMFT) calculations [5–7]. The $j_{eff} = 1/2$ picture brings Sr_2IrO_4 close to La_2CuO_4 electronically. Added to the structural similarity between the two materials, this analogy fostered the search for superconductivity by introducing carriers in the IrO_2 planes [4,8–13], and yet no superconductivity has been found so far. The reason may lie in the failures of the $j_{eff} = 1/2$ picture itself, and in fact several works started to dispute its validity. Doubts have arisen on both the form of the $j_{eff} = 1/2$ doublet [14–18] and the role of $j_{eff} = 3/2$ bands [19]. Possible experimental signatures of multiorbital effects were found under pressure [15] and strain [19]. Recent angle-resolved photoemission measurements show that Sr_2IrO_4 just sits marginally above the threshold for the spin-orbit coupling driven Mott insulator [20], and emphasize the presence of $j_{eff} = 3/2$ states close to the Fermi level [21]. The question of the validity of the effective one-band picture remains to date unsettled already at the theoretical level, however.

Even assuming that the $j_{eff} = 1/2$ picture is robust in the undoped case, it has still to be proven that it is preserved by doping and, if so, to what extent, a core question for

superconductivity. Theoretical studies of doping effects provided explanations for the formation of Fermi arcs and pseudogap [22], but have not clarified this point thus far. Experimentally, electron doping in Sr_2IrO_4 has been realized by partially replacing Sr with La [11,23,24], hydrogen irradiation [25], or by deposition of alkali metals on the surface [10,12]. Instead, hole doping has been obtained by replacing, e.g., Ir with Rh or Ru [20,26–32]. Such chemical substitution leads to unintentional effects besides the band filling, because of both the changes in the rotation of IrO_6 octahedra [27] and the differences in the ions themselves. These effects might result in local nonmagnetic Rh^{3+}-Ir^{5+} pairs [28,31], effectively weak spin-orbit coupling [20,26,27], and a Fermi surface that loses a large amount of its Ir 5d character [32]. In order to prove the robustness of the $j_{eff} = 1/2$ picture, it is of primary importance to separate the intrinsical effects of doping from all other factors, and show that, at least in principle, the scenario holds.

In this Letter we use the power of theoretical tools to clarify the two fundamental issues discussed above: (i) the role played by multiorbital effects in the undoped and doped cases and (ii) the intrinsical effects of doping. To this end we perform local-density approximation plus dynamical mean-field theory (LDA + DMFT) calculations without making any assumptions on the occupation and the form of the $j_{eff} = 3/2$ quartet and $j_{eff} = 1/2$ doublet. Our first conclusion is that the actual form of the $j_{eff} = 1/2$ states changes surprisingly little with $|x|$, the number of holes

036504-1

($x > 0$) or electrons ($x < 0$) in the IrO$_2$ plane. It is also weakly dependent on the exact value of the Coulomb repulsion. At first glance, this confers robustness to the $j_{\rm eff} = 1/2$ picture. Further analysis of the data shows, however, that the Mott gap ($x = 0$) is strongly reduced by the inter-$j_{\rm eff}$ couplings. This is a signature of the intrinsic three-band nature of the system and explains at the same time why the gap is small even for a relatively large average Coulomb repulsion—in relation to the $j_{\rm eff} = 1/2$ bandwidth. Upon hole doping, we find that the $j_{\rm eff} = 1/2$ picture starts to break down already at $x = 0.05$ holes, with half of the holes going in the $j_{\rm eff} = 3/2$ channels. The breakdown is evidenced by comparing to results for the ideal one-band model and looking at properties probing the low-energy spectrum.

In order to obtain these results, we first calculate the electronic structure of undoped Sr$_2$IrO$_4$ via the full-potential linearized augmented plane-wave method implemented in the WIEN2k code [33]. We adopt the local-density approximation and include the spin-orbit interaction in the calculation. Then we build the t_{2g} Wannier orbitals based Hubbard Hamiltonian,

$$\hat{H} = -\sum_{ii'}\sum_{mm'}\sum_{\sigma\sigma'} t^{i,i'}_{m\sigma,m'\sigma'}\hat{c}^{\dagger}_{im\sigma}\hat{c}_{i'm'\sigma'}$$
$$+\frac{1}{2}\sum_{i}\sum_{mm'pp'}\sum_{\sigma\sigma'} U_{mm'pp'}\hat{c}^{\dagger}_{im\sigma}\hat{c}^{\dagger}_{im'\sigma'}\hat{c}_{ip'\sigma'}\hat{c}_{ip\sigma}, \quad (1)$$

where $\hat{c}_{im\sigma}$ ($\hat{c}^{\dagger}_{im\sigma}$) annihilates (creates) an electron at lattice site i with orbital $m \in \{xy, yz, xz\}$ and spin $\sigma \in \{\uparrow, \downarrow\}$. The terms $-t^{i,i'}_{m\sigma,m'\sigma'}$ give the on-site crystal-field matrix ($i = i'$) and intersite hopping integrals ($i \neq i'$). We define $\varepsilon_{xy}, \varepsilon_{yz}, \varepsilon_{xz}$ the on-site energies and $\varepsilon_{\rm CF} = (\varepsilon_{yz} + \varepsilon_{xz})/2 - \varepsilon_{xy}$ the crystal-field splitting; λ_x and λ_y are the on-site spin-orbit couplings between xy and xz/yz orbitals, λ_z between yz and xz orbitals, and $\lambda = (\lambda_x + \lambda_y + \lambda_z)/3$ is the average spin-orbit coupling. The parameters $U_{mm'pp'}$ are elements of the screened Coulomb interaction tensor. The essential terms are [34] the direct Coulomb interaction, $U_{mm'mm'} = U_{m,m'} = U - 2J(1 - \delta_{m,m'})$, the exchange Coulomb interaction $U_{mm'm'm} = J$, the pair-hopping term, $U_{mmm'm'} = J$, and the spin-flip term $U_{mm'm'm} = J$. We solve the model with dynamical mean-field theory using the interaction-expansion continuous time quantum Monte Carlo impurity solver. More details on our implementation can be found in Refs. [35–37]. For the experimental structure [38] we get $\lambda_{x/y} \sim 346$ meV, $\lambda_z \sim 354$ meV, and $\varepsilon_{\rm CF} \sim 213$ meV from LDA calculations. The Coulomb parameters $U = 3.2$ eV and $J = 0.4$ eV can well produce the small experimental insulating gap [1,39], estimated as 0.1–0.6 eV. The $j_{\rm eff} = 1/2$ doublet is defined as

$$\left|\frac{1}{2},\sigma\right\rangle_{\rm eff} = i\alpha_2|xy,\sigma\rangle - \frac{\alpha_1}{\sqrt{2}}(|xz,-\sigma\rangle - 2i\sigma|yz,-\sigma\rangle), \quad (2)$$

where α_1 and α_2 are positive numbers, with $\alpha_1^2 + \alpha_2^2 = 1$, and where $|m,\sigma\rangle$ is a state with one hole in the m orbital. In the atomic limit with no crystal-field splitting, $\alpha_1 = \sqrt{(2/3)} \sim 0.82$. LDA yields a larger value, $\alpha_1 \sim 0.90$, which is also the value obtained by diagonalizing the DMFT occupation matrix in the undoped case. The $j_{\rm eff} = 1/2$ doublet Eq. (2) yields the occupations $n_{xy} = 1 + \alpha_1^2$, and $n_{xz} = n_{yz} = 2 - \frac{1}{2}\alpha_1^2$; thus, in the ideal case, $n_{xz} = n_{yz} = n_{xy} = 5/3$.

The first remarkable result of our calculations is that the coefficient α_1 depends weakly on $|x|$, the number of holes or (extra) electrons; more specifically, α_1 slightly decreases with increasing $|x|$, taking the value $\alpha_1 \sim 0.88$ for $x = -0.1$ and $\alpha_1 \sim 0.86$ for $x = 0.4$. The coefficient also depends little on the Coulomb repulsion, as shown in the Supplemental Material [40]. This result supports the $j_{\rm eff} = 1/2$ picture. In fact, a strong x and U dependence of α_1 would require a three-band model to determine the proper $j_{\rm eff} = 1/2$ doublet. This in turn would affect the strength of the effective intra-$j_{\rm eff} = 1/2$ bandwidth $\mathcal{W}_{\rm eff}$ and the associated Coulomb repulsion $\mathcal{U}_{\rm eff}$ [40,41]. For the closest neighbors, in first approximation the hopping integrals are $t_{\rm eff} = t(1 - \alpha_1^2/2)$, where $t = t_{xy,xy}$, while $t_{xz,xz} \sim t\langle\hat{\gamma}|\hat{x}\rangle$ and $t_{yz,yz} \sim t\langle\hat{\gamma}|\hat{y}\rangle$ for a bond along direction $\hat{\gamma} = \hat{x}, \hat{y}$. Thus $\mathcal{W}_{\rm eff}$ decreases with increasing α_1. Instead, the effective Coulomb repulsion is $\mathcal{U}_{\rm eff} = U - J(4 - 3\alpha_1^2)\alpha_1^2$ and has the minimum value, $\mathcal{U}_{\rm eff} = U - 4J/3$, for the ideal $j = 1/2$ state ($\alpha_1 = \sqrt{(2/3)}$). The dependence on α_1 does not cancel out in the $\mathcal{W}_{\rm eff}/\mathcal{U}_{\rm eff}$ ratio, the indicator of the strength of correlation effects. In fact, in the tight-binding approximation, setting $W = 8t$, the exact $j_{\rm eff} = 1/2$ limit [40] yields

$$R_{\rm eff} = \frac{\mathcal{W}_{\rm eff}}{\mathcal{U}_{\rm eff}} \sim \frac{W}{U}\frac{1 - \alpha_1^2/2}{1 - \frac{J}{U}(4 - 3\alpha_1^2)\alpha_1^2}, \quad (3)$$

which is about $0.72W/U$ for $J/U \sim 0.125$ and $\alpha_1 \sim 0.9$, the values from DMFT calculations.

Building on this key conclusion, i.e., on the fact that α_1 weakly depends on x and U, we will discuss the remaining results in a rigid $j_{\rm eff}$-basis picture. Figures 1 and 2 illustrate the principal outcomes. Figure 1 shows the distribution of holes in the different channels. In the undoped case ($x = 0$), the two $j_{\rm eff} = 3/2$ doublets are full and exhibit similar spectral functions (Fig. 2). The bottom panel of Fig. 1 shows that, correspondingly, the Coulomb enhancement of the spin-orbit coupling $\Delta\lambda(\omega)$ is much larger than the crystal-field splitting enhancement $\Delta\varepsilon_{\rm CF}(\omega)$. Introducing carriers (or decreasing the value of U [40]) thus makes the two $j_{\rm eff} = 3/2$ channels slightly anisotropic in comparison; this is more visible at low energy. Furthermore, since the
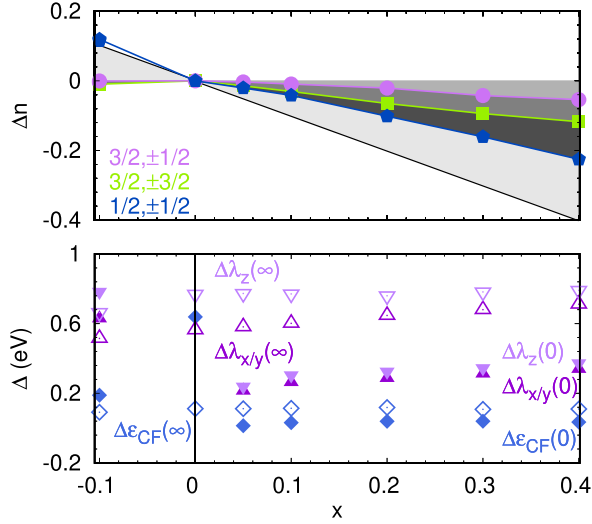
FIG. 1. Top: change in the occupations $\Delta n = n(x) - n(0)$ of the components of the j_{eff} Kramers states for $N = 5 - x$ electrons, as a function of the number of extra carriers x. Black line: ideal $j_{\text{eff}} = 1/2$ picture. Bottom: Coulomb enhancements [36] of crystal-field splitting, $\varepsilon_{\text{CF}} \to \varepsilon_{\text{CF}} + \Delta\varepsilon_{\text{CF}}(\omega)$, and spin-orbit couplings, $\lambda_\gamma \to \lambda_\gamma + \Delta\lambda_\gamma(\omega)$, for $\omega = 0$ (full symbols) and $\omega = \infty$ (empty symbols). Parameters are $U = 3.2$ eV, $J = 0.4$ eV, $T = 290$ K. The value $x = 0$ marks a discontinuity (vertical line), since at this point the system is a Mott insulator; here some enhancements become very large and out of scale.

FIG. 2. Top: LDA spectral functions, $x = 0$. Remaining panels: DMFT spectral functions in the j_{eff} basis for different x. Parameters are $U = 3.2$ eV and $J = 0.4$ eV, $T = 290$ K.

form of the j_{eff} doublet is almost x independent, upon doping a strong electron-hole asymmetry arises. Extra electrons go preferably into the $j_{\text{eff}} = 1/2$ channel; holes, however, go as likely into the $j_{\text{eff}} = 3/2$ states. This may be seen in the top panel of Fig. 1; the black line shows the occupation expected in the ideal $j_{\text{eff}} = 1/2$ picture. Figure 1 also shows that, within the $j_{\text{eff}} = 3/2$ quartet, holes prefer the $m_j = \pm 3/2$ states, those with no xy components.

The fact that multiband effects immediately emerge upon hole doping, as we have just established, appears at odds with the conclusion that, instead, in the $x = 0$ limit, fluctuations from the $j_{\text{eff}} = 3/2$ quartet to the $j_{\text{eff}} = 1/2$ doublet are totally suppressed. Further analysis, however, brings to light hidden multiband effects already present for $x = 0$. In Fig. 3 we compare, for different x values, the $j_{\text{eff}} = 1/2$ spectral function obtained from the three-band calculation with that obtained for an idealized model in which the $j_{\text{eff}} = 3/2$ bands are frozen. In the latter case the effective interaction strength is $\mathcal{U}_{\text{eff}} \sim U - 4J/3$, as we discussed above. When $|x|$ is very large, Hubbard bands are suppressed, similarly to the case of cuprates [42,43], and the differences between the results from the two models mostly amount to a shift in the chemical potential. Decreasing $|x|$ the spectral functions start to substantially differ, as can be seen from the positions of the Hubbard bands. Eventually, for $x = 0$, the gap E_g is sizably larger in the one-band calculation.
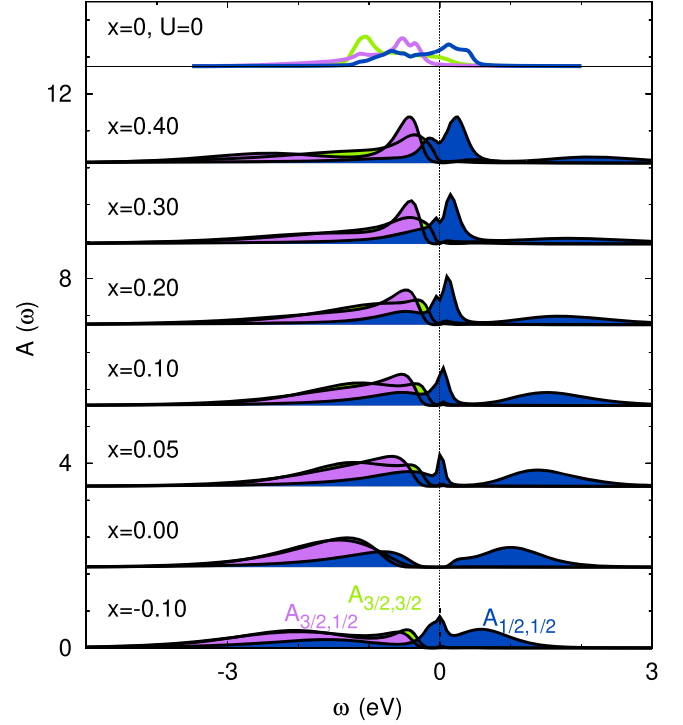
This can be understood as follows. By definition, the gap is $E_g = E(N + 1) + E(N - 1) - 2E(N)$. In this expression, $E(N)$ is the energy of the N-electron ground state $|\Psi_G^N\rangle$; in the $j_{\text{eff}} = 1/2$ picture, the main contributions to such a state come from local multiplets with $n_{3/2} \sim 4$. Instead, $E(N \pm 1)$ is the energy of $|\Psi_{j_{\text{eff}}=1/2}^{N\pm 1}\rangle$, the lowest energy $N \pm 1$-electrons eigenstates for which $|\langle \Psi_{j_{\text{eff}}=1/2}^{N\pm 1} | \hat{c}_{j_{\text{eff}}=1/2}^{(\dagger)} | \Psi_G^N \rangle|^2 \neq 0$, where $\hat{c}_{j_{\text{eff}}=1/2}^{(\dagger)}$ creates or destroys a $j_{\text{eff}} = 1/2$ electron. These states, however, may carry holes in the $j_{\text{eff}} = 3/2$ quartet ($n_{3/2} < 4$), in particular on the $N - 1$-electron side. This has two reasons. First, the j_{eff} states are linear combinations of t_{2g} orbitals, so that the inter-j_{eff} hopping integrals are large [40]. Second, the t_{2g}^4 multiplet with $n_{3/2} = 4$ is not a Coulomb-tensor eigenstate. Both effects make the gap smaller. Inter-j_{eff} hopping integrals reduce E_g by enhancing the effective orbital degeneracy [44,45] within the $N \pm 1$-electrons manifold. The intermultiplets Coulomb couplings shift spectral weight to lower energy, an effect which increases with J. In fact, we find that setting to zero both non-density-density Coulomb j_{eff} couplings and inter-j_{eff} hopping integrals increases the distance between Hubbard bands and reduces their spread, in line with the one-band model limit.

What is most surprising here is that these multiband effects remain large even when spin-orbital fluctuations are fully suppressed in the N-electron ground state. This is due
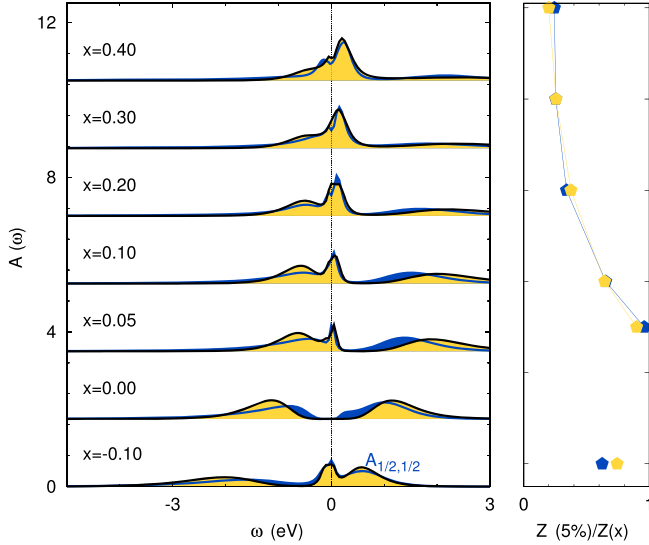
FIG. 3. Left: DMFT spectral function for the single- (yellow) and three- (blue) band model, for different x values. Right: change in inverse quasiparticle weight $Z(x)$ with increasing x.

FIG. 4. The in-plane optical conductivity (in $10^3 \, \Omega^{-1} \, \mathrm{cm}^{-1}$ units) for different x values. The panels show total, $j_{\mathrm{eff}} = 1/2$ intraorbital, and $j_{\mathrm{eff}} = 3/2$ intraorbital contributions and the rest. $U_{\mathrm{av}} = U - 2J$ is the average Coulomb interaction.

to the fact that many energy scales ($J, \varepsilon_{\mathrm{CF}}, \lambda$) are similar and hopping integrals between different j_{eff} states are large. The same conclusion can be derived from a three-orbital two-site toy model, as also shown in the Supplemental Material [40]. In fact, for the toy model one can see that the ideal $j_{\mathrm{eff}} = 1/2$ picture is only recovered for unrealistically large spin-orbit couplings, yielding the perfect $j_{\mathrm{eff}} - j_{\mathrm{eff}}$ coupling limit. In the Supplemental Material we show in addition that these conclusions hold also when accounting for possible changes in the octahedra rotation angle, e.g., induced by chemical doping.

The multiorbital effects just discussed can sizably increase $\mathcal{U}_c$, the critical U for the Mott transition in the $j_{\mathrm{eff}} = 1/2$ band. From the size of the gap for $x = 0$, we find that the enhancement factor is $r_c \sim 1.3$. This is further confirmed by the behavior of $1/Z$, the inverse quasiparticle weight obtained by introducing $|x|$ extra carriers, shown in the right-hand panel of Fig. 3. The value of $1/Z$ decreases approximately as $1/|x|$, as expected for a one-band doped Mott insulator. For $x > 0$, there are more $j_{\mathrm{eff}} = 1/2$ holes in the one-band than in the three-band case, however. Thus, everything else staying the same, for a given x for the one-band model the reduction should be larger than for the three-band model, in the $j_{\mathrm{eff}} = 1/2$ picture. Multiorbital effects roughly compensate the excess of holes, making Z rather similar for the two cases. Figure 3 shows that the spectral functions from the one- and three-band models are indeed similar at low energy, but not at high energy. In order to move the Hubbard bands to the same position as in the three-band model, $\mathcal{U}_{\mathrm{eff}}$ has to be reduced to $\mathcal{U}_{\mathrm{eff}}/r_c$; doing so, however, correspondingly reduces $1/Z$, e.g., for $x = 0.1$ approximately of the 23%. This shows that multi-band effects cannot be reproduced by statically screening $\mathcal{U}_{\mathrm{eff}}$ only.
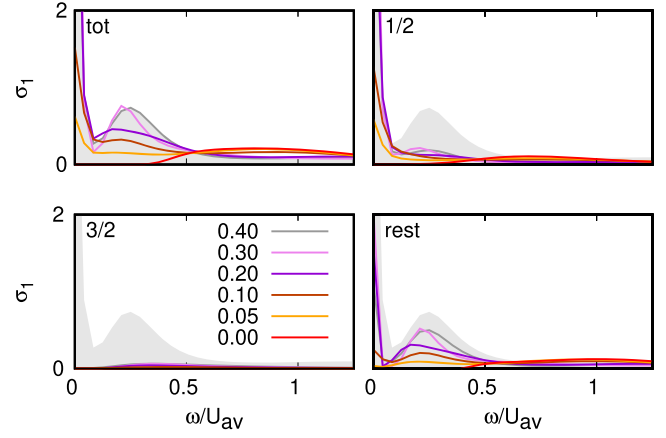
Finally, the positions of the Hubbard bands, the actual effective masses, and the presence of low-energy $j_{\mathrm{eff}} = 3/2$ states manifest themselves in low-energy probes as, e.g., the optical conductivity. The results for the latter are shown in Fig. 4. In this figure, we decompose the total in-plane optical conductivity into the contributions by intraorbital $j_{\mathrm{eff}} = 1/2$ ($\sigma_{1/2}$) and $j_{\mathrm{eff}} = 3/2$ ($\sigma_{3/2}$) terms and all multiorbital processes (σ_{rest}), $\sigma_{\mathrm{tot}} = \sigma_{1/2} + \sigma_{3/2} + \sigma_{\mathrm{rest}}$, following Ref. [41]. The figure shows that the peak at $\omega \sim 0.25 U_{\mathrm{av}}$ is directly controlled by multiorbital processes involving $j_{\mathrm{eff}} = 3/2$ states, and a sizable part of the Drude peak comes from the same processes. Even neglecting those, as we have seen, multiband effects affect the shape of the $j_{\mathrm{eff}} = 1/2$ spectral function, in particular, for small x, and thus deform the optical response.

Summarizing, we have studied multiband effects in doped $\mathrm{Sr_2IrO_4}$. We find that the shape of the effective $j_{\mathrm{eff}} = 1/2$ state is remarkably stable with increasing the number of extra carriers $|x|$ and the Coulomb repulsion U. This leads to electron-hole asymmetry: extra electrons go into the $j_{\mathrm{eff}} = 1/2$ channel, in line with experimental observations [10], while holes distribute into both the $j_{\mathrm{eff}} = 1/2$ and $j_{\mathrm{eff}} = 3/2$ channels, in contrast to expectations from the $j_{\mathrm{eff}} = 1/2$ picture. Most importantly, we find that the inter-j_{eff} coupling enhances $\mathcal{U}_c$, the effective single-band critical U for the Mott transition, keeping the undoped system on the verge of the metal-insulator transition for realistic Coulomb parameters. These results demonstrate the intrinsic three-band nature of doped iridates, putting into question one of the pillars on which the analogy with the cuprates is based. Similar conclusions are likely to apply to many other $4d$ and $5d$ spin-orbit transition-metal oxides. As a final remark, our three-band model calculations show in addition that the crystal-field enhancement is relatively small and x independent. Instead, the enhancement of the spin-orbit couplings is large and its

value at zero frequency substantially differs from the high-energy Hartree-Fock limit. This could be important for understanding and designing large gap correlated topological insulators [46].

[1] B. J. Kim, H. Jin, S. J. Moon, J.-Y. Kim, B.-G. Park, C. S. Leem, J. Yu, T. W. Noh, C. Kim, S.-J. Oh, J.-H. Park, V. Durairaj, G. Cao, and E. Rotenberg, Phys. Rev. Lett. **101**, 076402 (2008).

[2] B. J. Kim, H. Ohsumi, T. Komesu, S. Sakai, T. Morita, H. Takagi, and T. Arima, Science **323**, 1329 (2009).

[3] H. Jin, H. Jeong, T. Ozaki, and J. Yu, Phys. Rev. B **80**, 075112 (2009).

[4] F. Wang and T. Senthil, Phys. Rev. Lett. **106**, 136402 (2011).

[5] C. Martins, M. Aichhorn, L. Vaugier, and S. Biermann, Phys. Rev. Lett. **107**, 266404 (2011).

[6] R. Arita, J. Kuneš, A. V. Kozhevnikov, A. G. Eguiluz, and M. Imada, Phys. Rev. Lett. **108**, 086403 (2012).

[7] H. Zhang, K. Haule, and D. Vanderbilt, Phys. Rev. Lett. **111**, 246402 (2013).

[8] H. Watanabe, T. Shirakawa, and S. Yunoki, Phys. Rev. Lett. **110**, 027002 (2013).

[9] Z. Y. Meng, Y. B. Kim, and H. Y. Kee, Phys. Rev. Lett. **113**, 177003 (2014).

[10] Y. K. Kim, O. Krupin, J. D. Denlinger, A. Bostwick, E. Rotenberg, Q. Zhao, J. F. Mitchell, J. W. Allen, and B. J. Kim, Science **345**, 187 (2014).

[11] A. de la Torre, S. McKeown Walker, F. Y. Bruno, S. Riccó, Z. Wang, I. Gutierrez Lezama, G. Scheerer, G. Giriat, D. Jaccard, C. Berthod, T. K. Kim, M. Hoesch, E. C. Hunter, R. S. Perry, A. Tamai, and F. Baumberger, Phys. Rev. Lett. **115**, 176402 (2015).

[12] Y. K. Kim, N. H. Sung, J. D. Denlinger, and B. J. Kim, Nat. Phys. **12**, 37 (2016).

[13] Y. Hu, X. Chen, S.-T. Peng, C. Lane, M. Matzelle, Z.-L. Sun, M. Hashimoto, D.-H. Lu, E. F. Schwier, M. Arita, T. Wu, R. S. Markiewicz, K. Shimada, X.-H. Chen, Z.-X. Shen, A. Bansil, S. D. Wilson, and J.-F. He, Phys. Rev. Lett. **123**, 216402 (2019).

[14] L. C. Chapon and S. W. Lovesey, J. Phys. Condens. Matter **23**, 252201 (2011).

[15] D. Haskel, G. Fabbris, M. Zhernenkov, P. P. Kong, C. Q. Jin, G. Cao, and M. van Veenendaal, Phys. Rev. Lett. **109**, 027204 (2012).

[16] M. Moretti Sala, S. Boseggia, D. F. McMorrow, and G. Monaco, Phys. Rev. Lett. **112**, 026403 (2014).

[17] D. D. Khalyavin and S. W. Lovesey, Phys. Rev. B **100**, 224415 (2019).

[18] J. Jeong, B. Lenz, A. Gukasov, X. Fabrèges, A. Sazonov, V. Hutanu, A. Louat, D. Bounoua, C. Martins, S. Biermann, V. Brouet, Y. Sidis, and P. Bourges, Phys. Rev. Lett. **125**, 097202 (2020).

[19] L. Engström, T. Pereg-Barnea, and W. Witczak-Krempa, Phys. Rev. B **103**, 155147 (2021).

[20] B. Zwartsenberg, R. P. Day, E. Razzoli, M. Michiardi, N. Xu, M. Shi, J. D. Denlinger, G. Cao, S. Calder, K. Ueda, J. Bertinshaw, H. Takagi, B. J. Kim, I. S. Elfimov, and A. Damascelli, Nat. Phys. **16**, 290 (2020).

[21] B. Zwartsenberg, R. P. Day, E. Razzoli, M. Michiardi, M. X. Na, G. Zhang, J. D. Denlinger, I. Vobornik, C. Bigi, B. J. Kim, I. S. Elfimov, E. Pavarini, and A. Damascelli, Phys. Rev. B **105**, 245130 (2022).

[22] See, e.g., A. Moutenet, A. Georges, and M. Ferrero, Phys. Rev. B **97**, 155109 (2018); H. Wang, S.-L. Yu, and J.-X. Li, Phys. Rev. B **91**, 165138 (2015); A. Hampel, C. Piefke, and F. Lechermann, Phys. Rev. B **92**, 085141 (2015).

[23] S. Peng, C. Lane, Y. Hu *et al.*, npj Quantum Mater. **7**, 58 (2022).

[24] K. Terashima, M. Sunagawa, H. Fujiwara *et al.*, Phys. Rev. B **96**, 041106(R) (2017).

[25] Y. Yamashita, G. Lim, T. Maruyama *et al.*, Phys. Rev. B **104**, L041111 (2021).

[26] J. S. Lee, Y. Krockenberger, K. S. Takahashi, M. Kawasaki, and Y. Tokura, Phys. Rev. B **85**, 035101 (2012).

[27] T. F. Qi, O. B. Korneta, L. Li, K. Butrouna, V. S. Cao, X. Wan, P. Schlottmann, R. K. Kaul, and G. Cao, Phys. Rev. B **86**, 125105 (2012).

[28] J. P. Clancy, A. Lupascu, H. Gretarsson, Z. Islam, Y. F. Hu, D. Casa, C. S. Nelson, S. C. LaMarra, G. Cao, and Y. J. Kim, Phys. Rev. B **89**, 054409 (2014).

[29] A. Louat, F. Bert, L. Serrier-Garcia, F. Bertran, P. LeFèvre, J. Rault, and V. Brouet, Phys. Rev. B **97**, 161109(R) (2018).

[30] A. Louat, B. Lenz, S. Biermann, C. Martins, F. Bertran, P. LeFèvre, J. E. Rault, F. Bert, and V. Brouet, Phys. Rev. B **100**, 205135 (2019).

[31] Y. Cao, Q. Wang, J. A. Waugh, T. J. Reber, H. Li, X. Zhou, S. Parham, S.-R. Park, N. C. Plumb, E. Rotenberg, A. Bostwick, J. D. Denlinger, T. Qi, M. A. Hermele, G. Cao, and D. S. Dessau, Nat. Commun. **7**, 11367 (2016).

[32] V. Brouet, P. Foulquier, A. Louat, F. Bertran, P. Le Fèvre, J. E. Rault, and D. Colson, Phys. Rev. B **104**, L121104 (2021).

[33] P. Blaha, K. Schwarz, G. K. H. Madsen, D. Kvasnicka, and J. Luitz, WIEN2k, *An Augmented Plane Wave + Local Orbitals Program for Calculating Crystal Properties* (Technische Universität Wien, Wien, 2001); P. Blaha, K. Schwarz, P. Sorantin, and S. Trickey, Comput. Phys. Commun. **59**, 399 (1990).

[34] For a pedagogical presentation see, e.g., E. Pavarini, The LDA + DMFT approach, in *The LDA + DMFT Approach to Strongly Correlated Materials*, Vol. 1, edited by E. Pavarini, E. Koch, D. Vollhardt, and A. Lichtenstein (Forschungszentrum Jülich, Jülich, 2011).

[35] E. Gorelov, M. Karolak, T. O. Wehling, F. Lechermann, A. I. Lichtenstein, and E. Pavarini, Phys. Rev. Lett. **104**, 226401 (2010).

[36] G. Zhang, E. Gorelov, E. Sarvestani, and E. Pavarini, Phys. Rev. Lett. **116**, 106402 (2016); As discussed in this work, Coulomb enhancements of the on-site parameters are obtained from the self-energy, $\Delta\varepsilon_{CF} = \mathrm{Re}(\Sigma_{xz/yz\sigma} - \Sigma_{xy\sigma})$, $\Delta\lambda_z = 2\mathrm{Im}\Sigma_{xz\uparrow,yz\uparrow}$, $\Delta\lambda_x = -2\mathrm{Im}\Sigma_{xy\uparrow,xz\downarrow}$, $\Delta\lambda_y = 2\mathrm{Re}\Sigma_{xy\uparrow,yz\downarrow}$.

[37] G. Zhang and E. Pavarini, Phys. Rev. B **95**, 075145 (2017).

[38] T. Shimura, Y. Inaguma, T. Nakamura, M. Itoh, and Y. Morii, Phys. Rev. B **52**, 9143 (1995).

[39] J. Dai, E. Calleja, G. Cao, and K. McElroy, Phys. Rev. B **90**, 041102(R) (2014).

[40] See Supplemental Material at http://link.aps.org/supplemental/10.1103/PhysRevLett.131.036504 for more details.

[41] G. Zhang and E. Pavarini, Phys. Rev. B **99**, 125102 (2019). The actual value of $\mathcal{U}_{eff}$ is slightly larger, because the $j_{eff} = 1/2$ state is slightly different than the ideal $j = 1/2$ state. See Supplemental Material [40].

[42] J. Musshoff, A. Kiani, and E. Pavarini, Phys. Rev. B **103**, 075136 (2021).

[43] E. Pavarini, Riv. Nuovo Cimento **44**, 597 (2021).

[44] E. Koch, O. Gunnarsson, and R. M. Martin, Phys. Rev. B **60**, 15714 (1999).

[45] It should be noted that for the LDA bands alone, the inter-j_{eff} hopping integrals slightly reduce the $j_{eff} = 1/2$ bandwidth; everything else being the same, in a bare one-band picture this would correspondingly slightly increase the gap, the opposite of the effect we discuss here.

[46] J. Li, Q. Yao, L. Wu, Z. Hu, B. Gao, X. Wan, and Q. Liu, Nat. Commun. **13**, 919 (2022).

[47] www.gauss-centre.eu.